THE JOURNAL OF BIOLOGICAL CHEMISTRY VOL. 288, NO. 17, pp. 11920–11929, April 26, 2013
Published in the U.S.A.

Voltage-dependent Anion Channels Modulate Mitochondrial Metabolism in Cancer Cells

REGULATION BY FREE TUBULIN AND ERASTIN[*][S]

Received for publication, November 4, 2012, and in revised form, February 19, 2013 Published, JBC Papers in Press, March 7, 2013, DOI 10.1074/jbc.M112.433847

Eduardo N. Maldonado[‡§¶1], Kely L. Sheldon[‖], David N. DeHart[‡§], Jyoti Patnaik[‡§], Yefim Manevich[‡‡], Danyelle M. Townsend[§¶], Sergey M. Bezrukov[‖], Tatiana K. Rostovtseva[‖], and John J. Lemasters[‡§¶§§2]**

*From the [‡]Center for Cell Death, Injury & Regeneration, Departments of [§]Drug Discovery & Biomedical Sciences, [§§]Biochemistry & Molecular Biology, [‡‡]Cell & Molecular Pharmacology and Experimental Therapeutics, and [¶]Hollings Cancer Center, Medical University of South Carolina, Charleston, South Carolina 29425, the [‖]Program in Physical Biology, Eunice Kennedy Shriver National Institute of Child Health & Human Development, National Institutes of Health, Bethesda, Maryland 20892-2425, and **W. Harry Feinstein Department of Molecular Microbiology & Immunology, Bloomberg School of Public Health, Johns Hopkins University, Baltimore, Maryland 21205*

Background: Metabolites generating mitochondrial membrane potential ($\Delta\Psi$) enter through voltage-dependent anion channels (VDAC).
Results: VDAC3 contributed to $\Delta\Psi$ formation more than VDAC1/2. VDAC3 knockdown decreased ATP and NADH/NAD^+. Tubulin decreased VDAC1/2 not VDAC3 conductance, an effect antagonized by erastin.
Conclusion: Tubulin negatively modulates mitochondrial metabolism by closing VDAC1/2.
Significance: Antagonism of tubulin-dependent VDAC closure reverses mitochondrial suppression in Warburg metabolism.

Respiratory substrates and adenine nucleotides cross the mitochondrial outer membrane through the voltage-dependent anion channel (VDAC), comprising three isoforms — VDAC1, 2, and 3. We characterized the role of individual isoforms in mitochondrial metabolism by HepG2 human hepatoma cells using siRNA. With VDAC3 to the greatest extent, all VDAC isoforms contributed to the maintenance of mitochondrial membrane potential, but only VDAC3 knockdown decreased ATP, ADP, NAD(P)H, and mitochondrial redox state. Cells expressing predominantly VDAC3 were least sensitive to depolarization induced by increased free tubulin. In planar lipid bilayers, free tubulin inhibited VDAC1 and VDAC2 but not VDAC3. Erastin, a compound that interacts with VDAC, blocked and reversed mitochondrial depolarization after microtubule destabilizers in intact cells and antagonized tubulin-induced VDAC blockage in planar bilayers. In conclusion, free tubulin inhibits VDAC1/2 and limits mitochondrial metabolism in HepG2 cells, contributing to the Warburg phenomenon. Reversal of tubulin-VDAC interaction by erastin antagonizes Warburg metabolism and restores oxidative mitochondrial metabolism.

Non-proliferating tissues under aerobic conditions generate about 5% of cellular ATP through glycolysis and the remainder by mitochondrial oxidative phosphorylation. By contrast, cancer cells exhibit enhanced aerobic glycolysis and suppression of mitochondrial metabolism, as first described by Otto Warburg in the 1920s and referred to as the Warburg phenomenon (1, 2). Accordingly in aerobic cancer cells, glycolysis accounts for 50 to 70% of total cellular ATP production (3). In addition to ATP generation, enhanced glycolysis provides NADPH from the pentose shunt and carbon backbones for synthesis of lipids, proteins, and nucleotides for biomass formation during cell proliferation (4). The relevance of Warburg metabolism for cancer cell proliferation is well established, since augmentation of oxidative phosphorylation and/or inhibition of glycolysis promote cancer cell death both *in vivo* and *in vitro* (5–7).

Although Warburg suggested that what we now call oxidative phosphorylation is damaged in cancer cells, isolated tumor mitochondria are actually fully functional with regards to respiration and ATP synthesis (8). Moreover, mitochondria of cancer cells maintain mitochondrial membrane potential ($\Delta\Psi$) through respiration and ATP hydrolysis as predicted by chemiosmotic theory (9). Thus, suppression of mitochondrial metabolism in tumor cells is not a deficit of mitochondrial function but rather a physiological adaptation that remains incompletely understood. Oxidative phosphorylation requires flux of ATP, ADP, P_i, and respiratory substrates into and out of mitochondria. These hydrophilic metabolites cross the mitochondrial outer membrane via voltage-dependent anion channels (VDAC)[3] (10–13). VDAC is a highly conserved pore-forming 32 kDa protein comprising three isoforms in humans: VDAC1,

* This work was supported, in part, by Grants DK37034 and DK073336 from the National Institutes of Health. This work was also supported by the Intramural Research Program of the Eunice Kennedy Shriver National Institute of Child Health and Human Development (to K. L. S., S. M. B., and T. K. R).
[S] This article contains supplemental Figs. S1–S3.
[1] Recipient of a Specialized Program of Research Excellence Career Development Award (Grant P50 CA058187).
[2] To whom correspondence should be addressed: Center for Cell Death, Injury & Regeneration, Departments of Drug Discovery & Biomedical Sciences and Biochemistry & Molecular Biology, Medical University of South Carolina, DD504 Drug Discovery Building, 70 President St., MSC 140, Charleston, SC 29425. Fax: 843-876-2353; E-mail: JJLemasters@musc.edu.

[3] The abbreviations used are: VDAC, voltage-dependent anion channel; CCCP, carbonylcyanide *m*-chlorophenylhydrazine; TMRM, tetramethylrhodamine methylester; DPhPC, diphytanoyl phosphatidylcholine.

VDAC2, and VDAC3 encoded by separate genes. VDAC1 is the most abundant and best studied of the VDAC isoforms. VDAC1 forms a membrane-embedded β-barrel with an N terminus α-helix positioned inside the channel lumen as revealed by its crystal structure (14–16). In the open state, VDAC1 forms an aqueous channel of ~2.5 nm in internal diameter that is permeable to molecules up to ~5 kDa for nonelectrolytes, whereas pore diameter decreases to 1.8 nm in the closed state (17–20). VDAC is gated by voltage and shows ion selectivity. VDAC in its open state is permeable to ATP, ADP, and respiratory substrates. Although VDAC is generally considered to be constitutively open in aerobic cells, partial closure of VDAC has been proposed to account, in part, for the suppression of mitochondrial metabolism in the Warburg phenomenon (9, 21, 22).

Dimeric $\alpha\beta$-tubulin at nanomolar concentrations blocks VDAC conductance to make VDAC virtually impermeable to ATP (23). Free dimeric tubulin also suppresses respiration in isolated mitochondria and permeabilized cells by limiting mitochondrial entry of respiratory substrates, ADP and P_i for oxidative phosphorylation (23–25). In HepG2 human hepatoma and other cancer cells increased free tubulin decreases mitochondrial $\Delta\Psi$, which implies that free tubulin promotes VDAC closure in intact tumor cells (9). Accordingly, VDAC closure by free tubulin may contribute to suppression of mitochondrial metabolism in the Warburg phenomenon (9, 21, 26).

Erastin is a VDAC-binding small molecule that is selectively lethal to some cancer cells (27). It has been reported that erastin decreases the rate of NADH oxidation in isolated yeast mitochondria expressing a single mouse VDAC isoform (27) and that erastin increases permeance of NADH into liposomes containing human VDAC2 (28). However, the effects of erastin on VDAC function remain poorly understood.

Here, we evaluate the role of specific VDAC isoforms in mitochondrial metabolism by HepG2 cells and the effect of erastin on tubulin-VDAC interactions. Our results show that endogenous free tubulin in intact HepG2 cells decreases conductance of VDAC1 and VDAC2. Rather, conductance of the minor isoform VDAC3, which is relatively insensitive to tubulin, is most important for maintenance of mitochondrial $\Delta\Psi$, ATP generation, and redox state. We show also that erastin prevents and reverses tubulin-induced VDAC blockage both *in situ* and *in vitro* to promote mitochondrial metabolism and antagonize Warburg metabolism.

EXPERIMENTAL PROCEDURES

Materials—HepG2 cells and Eagle's minimum essential medium were purchased from American Tissue Culture Collection (Manassas, VA), AMP from Acros Organic (Pittsburgh, PA); ATP, ADP, carbonylcyanide *m*-chlorophenylhydrazine (CCCP), erastin, colchicine, myxothiazol, nocodazole, and paclitaxel from Sigma; diphytanoyl phosphatidylcholine from Avanti Polar Lipids (Alabaster, AL); tubulin from Cytoskeleton (Denver, CO); and tetramethylrhodamine methylester (TMRM) and Multispeck Multispectral Fluorescence Microscopy Standards kits from Invitrogen (Carlsbad, CA). All other reagents were analytical grade.

Cell Culture—HepG2 human hepatoma cells (American Type Culture Collection) were grown in Eagle's minimum essential medium supplemented with 10% fetal bovine serum, 100 units/ml penicillin and 100 μg/ml streptomycin in 5% CO_2/air at 37 °C. For confocal microscopy, cells were plated for 48 h on glass bottom culture dishes (MatTek, Ashland, MA). Live cell imaging was performed in 5% CO_2/air at 37 °C in modified Hank´s balanced salt solution (HBSS) containing (in mM): NaCl 137, Na_2HPO_4 0.35, KCl 5.4, KH_2PO_4 1, $MgSO_4$ 0.81, Ca_2Cl 0.95, glucose 5.5, $NaHCO_3$ 25, and HEPES 20, pH 7.4, as described (9).

siRNA Treatment and Real-time PCR—HepG2 cells grown to 70–80% of confluency were transfected with siRNA (5 nM) targeting VDAC1, VDAC2, and VDAC3 or control non-target siRNA (Ambion, Austin, TX). Non-target siRNA was Silencer Select Negative Control #1 siRNA (Catalogue #4390844). siRNAs for VDAC1, VDAC2, and VDAC3 were Silencer Select siRNAs: VDAC1, Catalogue #4390824, ID:s14769; VDAC2, Catalogue #4392420, ID:s14771; and VDAC3, Catalogue #4392420, ID:s230730. siRNAs were reverse transfected using Lipofectamine RNAiMAX Transfection Reagent according to the manufacturer's instructions (Invitrogen, Carlsbad, CA). mRNA levels of VDAC1, VDAC2, and VDAC3 were assessed by two-step quantitative polymerase chain reaction (qPCR). Total RNA was isolated using the Qiagen RNeasy Mini Kit (Qiagen, Valencia, CA) and quantified using a NanoDrop ND-1000 spectrophotometer (Nanodrop Technologies, Inc.). RNA was reverse transcribed into cDNA using a Bio-Rad iScript cDNA Synthesis kit. Primers for VDAC isoforms were designed using the Mfold webserver for nucleic acid folding prediction and Primer 3 for primer design. Forward and reverse primers were: 18S ribosomal RNA (r18S), GAG GGA GCC TGA GAA ACG G and GTC GGG AGT GGG TAA TTT GC; VDAC1, GGG TGC TCT GGT GCT AGG T and GAC AGC GGT CTC CA A CTT CT; VDAC2, CCA AAT CAA AGC TGA CAA GGA and TTT AGC TGC AAT GCC AAA AC; and VDAC3, TTG ACA CAG CCA AAT CCA AA and TGT TAC TCC CAG CTG TCC AA. qPCR was performed with a Bio-Rad MyiQ Single-Color Real-Time PCR Detection System using iQ SYBR Green Supermix (Bio-Rad). The abundance of VDAC isoforms was normalized to 18S rRNA by the $\Delta\Delta Ct$ method using Ct values obtained with MyiQ software.

Western Blots—Protein was quantified using bovine serum albumin as standard (Bio-Rad protein assay). Samples were separated on 4–12% NuPAGE Bis-Tris gels (Invitrogen) and transferred onto nitrocellulose membranes using an iBlot Dry Blotting System (Invitrogen). Blots were blocked for 60 min in 5% albumin and probed with antibodies against VDAC1 (SC-8828, Santa Cruz Biotechnologies, Santa Cruz, CA, 1:200); VDAC2 (Ab-47104, Abcam, Cambridge, MA, 1:500); VDAC3 (MSA03/E0836, MitoSciences, Eugene, OR, 1:1000); and β-actin (691002, MP Biomedicals, Solon, OH, 1:2000). Immunoblots were developed using secondary antibodies conjugated to peroxidase (Santa Cruz Biotechnology SC-2020 donkey anti-goat, SC-2004 goat anti-rabbit, and SC-2005 goat anti-mouse for VDAC1, VDAC2 and VDAC3 detection, respectively) at 1:3000. Detection was performed using a chemiluminiscence kit (Supersignal Westpico Chemiluminiscent Substrate, Rockford, IL).

Loading of Tetramethylrhodamine Methylester and Laser-scanning Confocal Microscopy—Cells in HBSS were loaded 30 min at 37 °C with 200 nM of TMRM. After loading and washing, subsequent incubations were performed with 50 nM TMRM to maintain equilibrium distribution of the fluorophore, as described (29). TMRM-loaded cells were incubated in HBSS in humidified 5% CO_2/air at 37 °C and imaged with a Zeiss LSM 510 NLO inverted laser scanning confocal/multiphoton microscope (Thornwood, NY) using 63× 1.4 N.A. planapochromat oil immersion lens, as described (9, 30). Fluorescence of TMRM was excited at 543-nm and detected through a 560-nm long-pass filter and a one Airy unit diameter pinhole. NADH autofluorescence was imaged using multiphoton laser excitation (720 nm, 15% power) and an infrared-blocking emission barrier filter (460 ± 25 nm).

Fluorescent polystyrene microspheres (4-μm, MultiSpeck Multispectral Fluorescence Microscopy Standards Kit M-7901, Molecular Probes, Invitrogen) were used as fiduciary markers. Microspheres were prediluted in HBSS and added to TMRM-loaded cells incubated in HBSS at a final concentration of 30,000/ml. Images were taken 20 min after addition to allow sedimentation of the microspheres.

TMRM fluorescence and NADH autofluorescence were quantified using Zeiss LSM and Photoshop CS4 (Adobe Systems, San Jose, CA) software. TMRM fluorescence and NADH autofluorescence were determined after subtraction of background of fluorescence images collected within the coverslip.

HPLC Detection and Quantification of Adenine Nucleotides—The incubation medium of HepG2 cells cultured in 6-well plates was replaced with 2.5% trichloroacetic acid (TCA) at 4 °C. After 3 min, the plates were scraped, and the extracts were centrifuged at 10,000 × *g* for 5 min at 4 °C. The supernatants were then diluted with water and neutralized with 0.1 M Tris acetate buffer. Adenine nucleotides in the extracts were quantified using a Waters Model 1525 Binary Breeze HPLC pump equipped with a Model 717 Plus Autosampler and a Model 2487 UV-Vis Detector (Waters, Milford, MA). Experiments were performed using a C_{18}, 5 μm, 4.6 × 150-mm reverse phase column (SunFire™, Waters), isocratic elution (1 ml/min) with 100 mM Na-phosphate buffer (pH 5.5), and detection at 260 nm. The TCA lysates (25 μl) were injected into the column, and ATP, ADP, and AMP were detected at approximate retention times of 4.1, 4.9, and 11.5 min, respectively. Authenticity of detection was confirmed by spiking actual samples with known amounts of ATP, ADP, and AMP as standards. Peak areas were quantified using Empower 2 software (Waters). Millimolar concentrations of adenine nucleotides and P_i were calculated based on measured protein/cell assuming a cell volume of 4000 fl (31).

Phosphate Determination—Inorganic phosphate in cellular extracts was determined with a Phosphate Colorimetric Assay Kit (BioVision, Mountain View, CA, Cat. #K410-500) according to the manufacturer's instructions.

Mitochondrial Fractions—HepG2 cells were trypsinized, and mitochondrial fractions were prepared using a Mitochondria/Cytosol Fractionation Kit (BioVision, Cat. #256-25) at 4 °C according to the manufacturer's instructions. The resulting crude mitochondrial fraction was stored at −20 °C for subsequent isolation of VDAC.

VDAC Isolation and Reconstitution—VDAC was isolated from HepG2 mitochondrial fractions and reconstituted into planar bilayer membranes of diphytanoyl phosphatidylcholine (DPhPC) across a 70–80 μm diameter aperture within a Teflon film separating two compartments containing 1 M KCl buffered with 5 mM Hepes at pH 7.4, as described with minor modifications (32). After VDAC channel insertion and measurement of VDAC parameters, bovine brain tubulin was added to one side of the planar bilayer under constant stirring for 1 min. As indicated erastin was added to both sides of the membrane under constant stirring.

Current recordings were performed using an Axopatch 200B amplifier (Axon Instruments, Foster City, CA) in the voltage clamp mode, as described (32). Potential was defined as positive when higher on the side of VDAC addition (*cis*). Multichannel experiments were carried out with an average of ~50 channels reconstituted into the planar bilayer. VDAC voltage-dependent properties were assessed following protocols developed previously in which gating is inferred from the channel response to a slowly changing periodic transmembrane voltage (5 mHz, ±60 mV) (33, 34). Data were collected and analyzed as previously described (32).

Statistics—Differences between groups were analyzed by the Student's *t* test using $p < 0.05$ as the criterion of significance. Data points are means of 3–6 independent experiments ± S.E. Images are representative of three or more independent experiments.

RESULTS

Isoform-specific siRNA Knockdown Selectively Decreases mRNA and Protein Expression of All VDAC Isoforms in HepG2 Human Hepatoma Cells—HepG2 cells expressed all three VDAC isoforms, as assessed by qPCR. VDAC2 (~49%) was the most abundant isoform, followed by VDAC1 (~40%) and VDAC3 (~11%) (Fig. 1*A*). Transfection with isoform-specific siRNAs (5 nM) targeting VDAC1/2/3 decreased corresponding VDAC mRNA levels by ~90% after 48 h without affecting mRNA expression of the other VDAC isoforms (Fig. 1*B* and data not shown). Immunoblotting also showed that siRNA treatment for 48 h selectively knocked down protein expression of the target VDAC isoforms by ~90% without affecting non-target VDAC isoforms (Fig. 1*B*).

VDAC Knockdown Decreases Mitochondrial Membrane Potential—Previously, increased cellular free tubulin induced by microtubule-destabilizing agents was shown to decrease mitochondrial $\Delta\Psi$, an effect attributed to free tubulin-dependent inhibition of VDAC permeability. To assess the effects of VDAC knockdown on $\Delta\Psi$, HepG2 cells were loaded with the mitochondrial $\Delta\Psi$-indicating fluorophore TMRM and imaged by confocal microscopy. In HepG2 cells treated with non-target siRNA, mitochondria strongly labeled with TMRM (Fig. 1*C*, *upper left panel*). Knockdown of VDAC isoforms 1, 2, and 3 decreased mitochondrial TMRM labeling by 42, 59, and 79%, respectively, compared with cells transfected with non-target siRNA (Fig. 1, *C* and *D*). The greatest decrease of $\Delta\Psi$ occurred after knockdown of VDAC3, the least abundant isoform. Fluo-

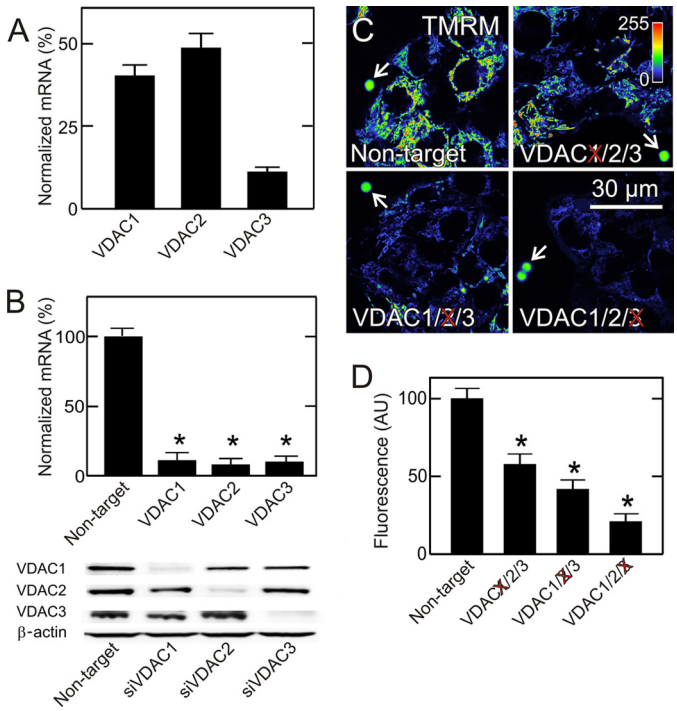

FIGURE 1. **VDAC knockdown decreases mitochondrial membrane potential in HepG2 cells.** In *A*, relative abundance of mRNA for VDAC1, VDAC2 and VDAC3 in native HepG2 cells was determined by qPCR. In *B*, cells were transfected with non-target siRNA and siRNA against VDAC1, VDAC2 and VDAC3. After 48 h, mRNA expression of the corresponding VDAC isoform and protein expression of all three isoforms were assessed by qPCR and immunoblotting. In *C* at 48 h after transfection with non-target siRNA and siRNA against VDAC1, VDAC2, and VDAC3, HepG2 cells were loaded with TMRM and imaged. Note decrease of mitochondrial TMRM fluorescence after knockdown of each VDAC isoform, but most markedly after VDAC3 knockdown. Image intensity was pseudocolored according to the reference bar. *Arrows* identify 4-μm fiduciary fluorescent beads. In *D*, average TMRM fluorescence after knockdown was plotted in comparison to transfection with non-target siRNA. *, $p < 0.05$ from five independent experiments analyzing 4–5 random fields containing 5–10 cells.

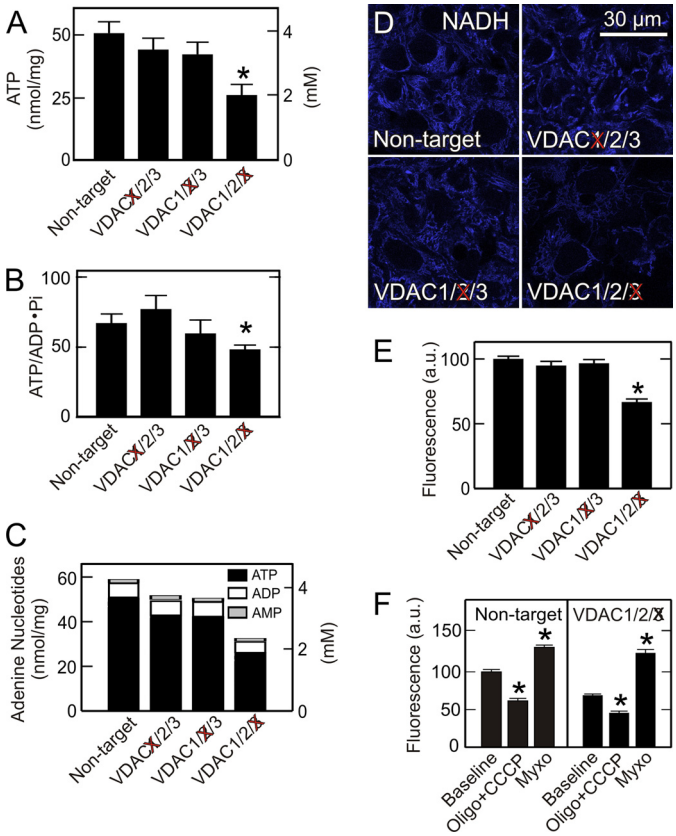

FIGURE 2. **VDAC3 knockdown decreases ATP, phosphorylation potential, adenine nucleotides, and NAD(P)H redox state.** In *A*--*C*, adenine nucleotides and phosphate in HepG2 cells were measured after siRNA knockdown of VDAC1, VDAC2, and VDAC3, as described under "Experimental Procedures." In *D*, NAD(P)H autofluorescence was imaged by multiphoton microcopy. Note that VDAC3 but not VDAC1 or VDAC2 knockdown decreased mitochondrial NADH autofluorescence. In *E*, average NAD(P)H autofluorescence after knockdown of VDAC isoforms is plotted in comparison to transfection with non-target siRNA. In *F*, NAD(P)H autofluorescence before and after addition of CCCP plus oligomycin or myxothiazol was measured for HepG2 cells transfected with non-target siRNA and siRNA against VDAC3. *, $p < 0.05$ compared with *Non-target* or *Baseline* from three independent experiments analyzing 4–5 random fields containing 5–10 cells.

rescent beads were used as fiduciary markers to standardize fluorescence between experiments (Fig. 1*C*, *arrows*).

VDAC3 Knockdown Decreases Cellular ATP and ADP—To determine if decreased VDAC expression affects cellular adenine nucleotide concentrations, we measured ATP, ADP, and AMP after single knockdown of the three VDAC isoforms. Despite downward trends, ATP and ADP after VDAC1 and VDAC2 knockdown were not statistically significantly different than after non-target siRNA treatment (Fig. 2*A* and supplemental Fig. S1). By contrast after VDAC3 knockdown, ATP and ADP were decreased significantly by 48 and 27%, respectively (Fig. 2*A* and supplemental Fig. S1). AMP, a precursor of ADP and ATP, remained unchanged after knockdown of each of the VDAC isoforms. Phosphate also was unchanged (supplemental Fig. S1). Energy charge also decreased after VDAC3 knockdown from 0.93 ± 0.02 after non-target siRNA treatment to 0.89 ± 0.02 ($p < 0.05$). Downward trends of energy charge after VDAC1 and VDAC2 knockdown were not statistically significant (data not shown). The ATP/ADP·P_i ratio, an indicator of the cellular phosphorylation potential, decreased by 40% after VDAC3 knockdown but not after knockdown of the other VDAC isoforms (Fig. 2*B*). In comparison to treatment with non-target siRNA, total adenine nucleotide levels were unchanged after knockdown of VDAC1 and VDAC2 but decreased by 45% after knockdown of VDAC3 (Fig. 2*C*). Overall, VDAC3 was the isoform most important for maintenance of ATP levels in HepG2 cells.

Knockdown of VDAC3 Decreases NADH and NADH Redox State—VDAC mediates entry of pyruvate, acyl-CoA and most other respiratory substrates into mitochondria. These substrates reduce NAD^+ to NADH. Accordingly, we assessed by multiphoton microscopy the effect of VDAC knockdown on mitochondrial NADH. Multiphoton fluorescence of reduced pyridine nucleotides, NADH and NADPH, arises almost exclusively from mitochondria, because fluorescence of NAD(P)H is highly quenched in the cytosol (35, 36). In comparison to treatment with non-target siRNA, knockdown of VDAC1 and VDAC2 caused no change of mitochondrial NAD(P)H fluorescence (Fig. 2, *D* and *E*). By contrast, VDAC3 knockdown decreased NAD(P)H fluorescence by 33% (Fig. 2, *D* and *E*).

We further characterized the effect of VDAC3 knockdown on mitochondrial NAD(P)H/$NAD(P)^+$ ratios. To estimate NAD(P)H, HepG2 cells after VDAC3 knockdown or non-target

siRNA treatment were exposed to an uncoupler (CCCP, 2 μM) plus an ATP synthase inhibitor (oligomycin, 10 μg/ml), the latter to prevent uncoupler-stimulated ATP hydrolysis. Uncoupler promotes nearly complete oxidation of NAD(P)H. Thus, the percentage decrease of autofluorescence after CCCP plus oligomycin treatment is proportional to NAD(P)H before the additions. This decrease after uncoupler was 41 and 22%, respectively, for non-target siRNA and VDAC3 knockdown (Fig. 2*F*). In parallel experiments, we inhibited respiration with myxothiazol (10 μM), a complex III respiratory inhibitor. Myxothiazol causes maximal reduction of mitochondrial $NAD(P)^+$, and thus the subsequent percentage increase of mitochondrial NAD(P)H autofluorescence is proportional to $NAD(P)^+$ prior to respiratory inhibition. This increase after myxothiazol was 33 and 65%, respectively, after non-target siRNA and VDAC3 knockdown. From these measurements, NAD(P)H/$NAD(P)^+$ ratios were 1.21 for non-target siRNA and 0.35 for VDAC3 knockdown. These findings indicate that VDAC3 is important for the influx of respiratory substrates that reduce NAD^+ in mitochondria of HepG2 tumor cells.

VDAC Knockdown Blunts Free Tubulin-induced Suppression of Mitochondrial Membrane Potential Formation—In cancer cells, free tubulin is a dynamic negative regulator of mitochondrial $\Delta\Psi$, and tubulin-induced inhibition of VDAC permeability is proposed as the mechanism underlying this regulation (9). To investigate the effects of VDAC isoform knockdown on free tubulin-induced changes of mitochondrial $\Delta\Psi$, HepG2 cells were treated with microtubule destabilizers and stabilizers to increase and decrease free tubulin, respectively. In cells transfected with non-target siRNA, nocodazole (10 μM), a microtubule destabilizer, decreased mitochondrial TMRM uptake from 100 to 31 arbitrary units (AU) (Fig. 3, *A* and *B*), similar to previous results in untreated HepG2 cells (9). To investigate whether the nocodazole-induced decrease of $\Delta\Psi$ was VDAC-dependent, VDAC isoform knockdowns were again performed. After siRNA treatment, TMRM uptake decreased to 56, 42, and 20 AU, respectively, after VDAC1, VDAC2, and VDAC 3 knockdown, as shown above (Fig. 1*D*). Nocodazole further diminished TMRM uptake to 33, 19, and 13 AU, respectively (Fig. 3*B*). Thus, all isoforms contributed to inhibition of $\Delta\Psi$ formation by free tubulin. In absolute terms, VDAC3 knockdown diminished the effect of nocodazole on $\Delta\Psi$ to the greatest extent. One interpretation of these results is that VDAC1 and VDAC2 are constitutively partially closed due to the blockage by endogenous free tubulin. Rather, VDAC3 is the VDAC isoform most constitutively open in wild type cells and least inhibited by endogenous free tubulin (Fig. 3, *A* and *B*). In the absence of VDAC3, only VDAC1 and VDAC2 are present. Since VDAC1 and VDAC2 are already inhibited by endogenous free tubulin, nocodazole has little effect.

To assess the effects of decreasing cellular free tubulin on $\Delta\Psi$ formation after VDAC knockdown, HepG2 cells were treated with the microtubule stabilizer, paclitaxel. Paclitaxel promotes microtubule polymerization and decreases free tubulin. After paclitaxel (10 μM), TMRM fluorescence increased from 100 to 152 AU in cells transfected with non-target siRNA (Fig. 3, *A* and *B*). A similar increase occurred in wild type cells (9). After knockdown of VDAC isoforms 1, 2, and 3, paclitaxel increased

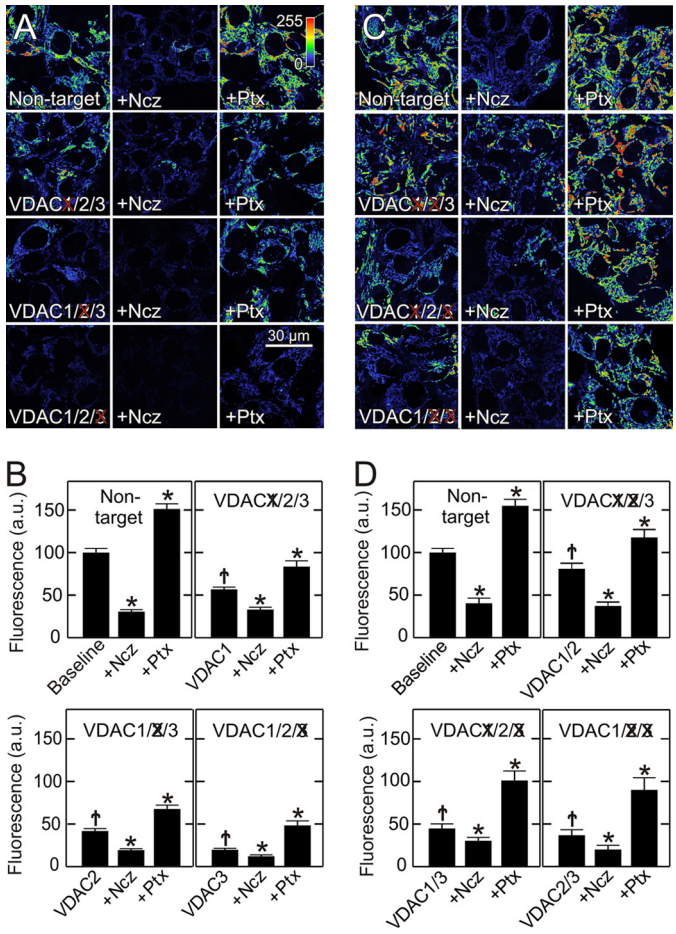

FIGURE 3. **Single and double VDAC knockdowns decrease mitochondrial membrane potential and alter responses to free tubulin.** HepG2 cells were loaded with TMRM at 48 h after siRNA transfection, as described in Fig. 1. In *A*, single knockdowns of VDAC isoforms were performed, which decreased TMRM fluorescence compared with cells transfected with non-target siRNA (*left panels*). To varying extents, nocodazole (Ncz, 10 μM) (*middle panels*) decreased TMRM uptake, whereas paclitaxel (Ptx, 10 μM) (*right panels*) increased fluorescence. Images were collected 30 min after treatment. In *B*, results of treatments described in *A* were quantified. In *C*, double knockdowns of VDAC isoforms were performed in all possible combinations. To different extents, VDAC double knockdowns decreased TMRM fluorescence (*left panels*). Note also that nocodazole (*middle panels*) decreased and paclitaxel (*right panels*) increased TMRM fluorescence as quantified in *D*. *, $p < 0.05$ from five independent experiments analyzing 4–5 random fields containing 5–10 cells. †, $p < 0.05$ compared with non-target baseline.

TMRM fluorescence from 56, 42, and 20 to 83, 68, and 48 AU, respectively (Fig. 3*A* and *B*). Although paclitaxel hyperpolarized mitochondria in VDAC1/2/3 knockdown cells, paclitaxel was unable to restore $\Delta\Psi$ to non-target levels.

VDAC Double Knockdown Isolates Individual VDAC Isoforms—To better characterize the contribution of each VDAC isoform to the inhibitory effect of free tubulin, VDAC double knockdowns were performed. Double knockdowns of VDAC isoforms in all three possible combinations decreased corresponding mRNA and protein expression by ~90 and ~80%, respectively, without changing expression levels of the non-target VDAC isoform (supplemental Fig. S2). In confirmation of the single knockdown findings, VDAC double knockdowns decreased mitochondrial $\Delta\Psi$ to different extents, and TMRM uptake decreased from 100 AU in cells transfected with non-target siRNA to 80, 45, and 37 AU, respectively, after dou-

ble knockdown of VDAC1/2, VDAC1/3, and VDAC2/3 (Fig. 3, *C* and *D*). The decrease of $\Delta\Psi$ was greatest when VDAC3 was knocked down in combination with either VDAC1 or VDAC2 and least in the VDAC1/2 double knockdown (Fig. 3, *C* and *D*). These double knockdown results support observations of single VDAC isoform knockdowns to indicate that the least abundant VDAC isoform, VDAC3, was most important quantitatively to sustain $\Delta\Psi$.

Double knockdown cells were also treated with nocodazole and paclitaxel. After nocodazole, mitochondrial TMRM fluorescence decreased from 81, 45, and 37 to 43, 14, and 17 AU, respectively, in VDAC1/2, VDAC1/3, and VDAC2/3 double knock-out cells (Fig. 3, *C* and *D*). By contrast, paclitaxel increased TMRM fluorescence to 118, 101, and 90 AU (Fig. 3, *C* and *D*). Thus, in VDAC1/2 double knockdown cells expressing predominantly VDAC3, the depolarizing effect of nocodazole was greatest, and the hyperpolarizing effect of paclitaxel was least in comparison to cells predominantly expressing VDAC1 (VDAC2/3 knockdown) or VDAC2 (VDAC1/3 knockdown). These results together with the findings with single VDAC isoform knockdowns support the conclusion that free tubulin maintains VDAC1 and VDAC2 in a mostly closed state under baseline conditions and that VDAC3 is less sensitive to tubulin and is constitutively in a mostly open state. Thus, the least abundant VDAC3 is the VDAC isoform most important for maintenance of mitochondrial metabolism in HepG2 cells.

VDAC Isolated from HepG2 Cells Forms Channels in Planar Lipid Membranes—When VDAC isolated from mitochondrial fractions of HepG2 cells was reconstituted into planar lipid membranes, typical VDAC channels were observed with single-channel conductances of ~4.2 nS in 1 M KCl, characteristic voltage-gating behavior and characteristic conductance *versus* voltage curves (supplemental Fig. S3, *A* and *B*). Addition of nanomolar free dimeric tubulin to the surrounding membrane buffer solution induced characteristic blockages of channel conductance, as described previously (24) (supplemental Fig. S3*C*). Thus, VDAC isolated from HepG2 mitochondria and reconstituted into a planar lipid membrane forms typical channels with the properties previously described for VDAC from other sources.

VDAC Isoforms Show Different Sensitivity to Blockage by Tubulin—To determine if free tubulin inhibition was specific for a particular VDAC isoform, VDAC was isolated from mitochondrial fractions of VDAC2/3, VDAC1/3, and VDAC1/2 double knockdown HepG2 cells to yield VDAC1, VDAC2, and VDAC3-enriched fractions, respectively. To obtain VDAC gating behavior representative of the majority of channels in each isoform-enriched fraction, experiments were performed on multi-channel membranes with an average of about 50 channels inserted, as described (32–34). During application of a slow periodic triangular voltage wave, channel closure at different potentials was expressed as conductance, G, normalized to maximal conductance, G_{max}, in each voltage wave period. For fractions enriched in each of the three VDAC isoforms, nearly identical dependences of normalized conductance *versus* voltage were obtained (Fig. 4*A*), which was identical to conductance of VDAC isolated from control wild type cells (supplemental Fig. S3*C*). An asymmetry of voltage gating with more pronounced closure at negative potentials is indicative of an intrinsic asymmetry of VDAC in which the channel has two different closed states depending on the sign of the applied voltage (24, 32, 33). Although the voltage gating was similar for the three VDAC-enriched fractions, the response to tubulin blockage was remarkably different. Tubulin (10 nM) enhanced the responses to voltage for VDAC1- and VDAC2-enriched fractions (isolated from VDAC2/3 and VDAC1/3 double knockdown HepG2 cells, respectively), whereas the same concentration of tubulin had virtually no effect on VDAC3-enriched fractions isolated from VDAC1/2 double knockdown cells (Fig. 4*B*). These results confirm that the VDAC species isolated from VDAC1/2 double knockdown cells is indeed different from that

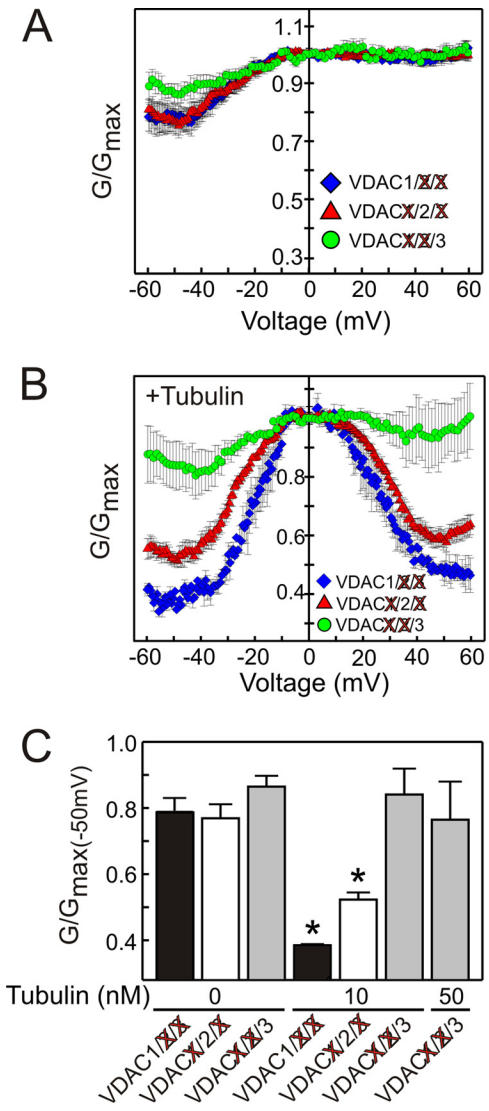

FIGURE 4. **VDAC 1, 2, and 3 isoforms have different sensitivity to blockade by tubulin.** Double knockdowns of VDAC isoforms were performed in all possible combinations in HepG2 cells, and the remaining VDAC isoform was isolated and inserted into lipid bilayers. In *A*, normalized average conductance, G/G_{max}, is plotted *versus* applied voltage for the three VDAC isoforms in the absence of tubulin. In *B*, tubulin (10 nM) was added to both sides of the membrane, which increased VDAC voltage-induced closure and decreased minimum conductance at $> \pm 40$ mV for VDAC1 and 2 but did not affect VDAC3. In *C*, normalized conductance at −50 mV was plotted for all VDAC isoforms at tubulin concentrations of 10 nM and 50 nM, as indicated. *, $p <$ 0.001 compared with no tubulin from 3–6 experiments for each group.

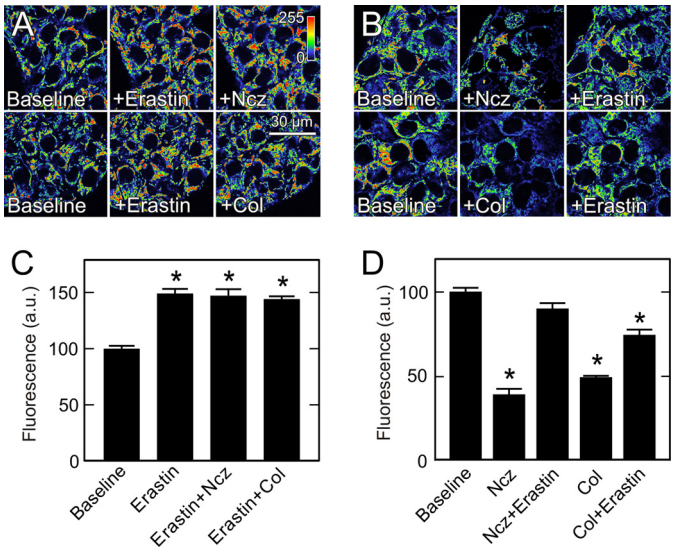

FIGURE 5. **Erastin increases mitochondrial membrane potential and blocks and reverses depolarization induced by free tubulin.** TMRM-loaded HepG2 cells were imaged, as described in Fig. 1. In *A*, cells were imaged before (*left panels*) and 30 min after treatment with erastin (10 μM) (*center panels*) and after 30 min treatment with erastin followed by 30 min treatment with nocodazole (Ncz, 10 μM) or colchicine (Col, 10 μM) (*right panels*). In *B*, cells were imaged before (*left panels*) and after treatment with nocodazole or colchicine for 30 min (*center panels*) followed by erastin for 30 min (*right panels*). In *C* and *D*, TMRM fluorescence after various treatments is compared with untreated cells (*Baseline*). *, $p < 0.05$ from four independent experiments analyzing 4–5 random fields containing 5–10 cells.

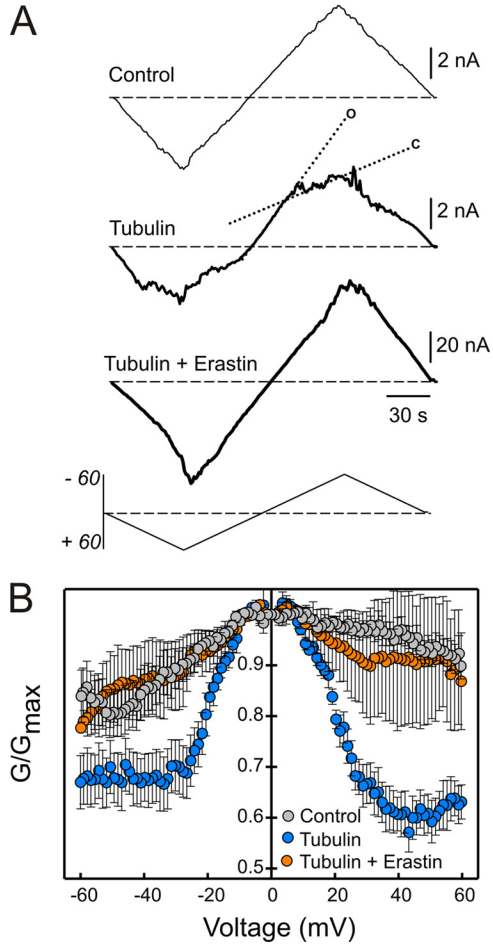

FIGURE 6. **Erastin reverses tubulin-induced blockage of VDAC in planar lipid membranes.** In *A*, representative current traces through the same multichannel membrane in response to periodic triangular voltage waves (± 60 mV, 5 mHz, *bottom of panel A*) were registered before (*trace a*) and after (*trace b*) addition of 50 nM tubulin followed by the addition of 50 μM of erastin (*trace c*). *Dotted lines* indicate a steep slope of high or open conductance at low voltages (**o**) and more gradual slope of low conductance (**c**) at higher voltages. In *B*, normalized average conductance *versus* voltage is plotted from three experiments as shown in *A* where erastin addition after tubulin restored VDAC voltage gating to the level observed in the absence of tubulin. Each data point is the mean of 3–6 experiments ± S.E.

isolated from VDAC1/3 and VDAC2/3 double knockdown cells.

The difference in tubulin sensitivity of the different VDAC isoforms is best illustrated in plots of tubulin-induced decreases of the normalized conductance, G/G_{max}, at −50 mV before and after addition of 10 nM tubulin (Fig. 4*C*). Tubulin at 50 nM was not enough to induce significant closure of VDAC3, whereas only 10 nM tubulin was enough to induce 50 and 32% decreases, respectively, of VDAC1 and VDAC2 conductance (Fig. 4, *B* and *C*). Tubulin at 50 nM was the maximum concentration tested because higher concentrations of tubulin induced massive VDAC insertions that eventually led to the membrane rupture. These data show that VDAC isoforms have different sensitivities to inhibition by tubulin: VDAC1 > VDAC2 ≫ VDAC3.

Erastin Blocks and Reverses the Effect of Free Tubulin on Mitochondrial Membrane Potential—Erastin is a VDAC-binding small molecule that is selectively lethal to cancer cells (27). Accordingly, we investigated whether erastin affected the interaction of tubulin with VDAC. Treatment of HepG2 cells with erastin (10 μM) increased mitochondrial TMRM uptake from 100 to 149 AU (Fig. 5, *A* and *C*). Although colchicine and nocodazole strongly decreased mitochondrial $\Delta\Psi$ (see Fig. 3, *B* and *D*), pretreatment with erastin (10 μM) abrogated completely mitochondrial depolarization induced by nocodazole and colchicine (Fig. 5, *A*, *right panels*, and *C*). Moreover, when cells were first treated with nocodazole or colchicine to depolarize mitochondria to 39 and 49 AU, respectively, subsequent erastin (10 μM) restored mitochondrial TMRM uptake to 90 and 74 AU (Fig. 5, *B* and *D*). These findings show that erastin can both prevent and reverse free tubulin-dependent inhibition of mitochondrial $\Delta\Psi$ formation.

Erastin Antagonizes Blockage of VDAC Conductance by Tubulin—The effects of erastin on tubulin-dependent changes of mitochondrial $\Delta\Psi$ suggested that erastin was preventing tubulin-induced blockage of VDAC conductance. To address directly effects of erastin on VDAC conductance, VDAC from wild type HepG2 cells was reconstituted into planar membranes in the presence and absence of tubulin and/or erastin. Tubulin (50 nM) decreased multichannel current at high positive and negative potentials (>40 mV), signifying a tubulin-induced decrease of VDAC conductance (Fig. 6*A*, compare *upper [control] and middle traces*). In the middle trace, dotted lines indicate slopes of high or open conductance (**o**) and low or closed conductance (**c**). Erastin (50 μM) added after tubulin completely abolished the effects of tubulin and restored a current-voltage profile that was essentially identical to that observed in the absence of tubulin (Fig. 6*A*, *lower trace*). When added alone in the absence of tubulin, erastin had no effect on the current-voltage profile for VDAC (data not shown). Thus,

the effect of erastin on VDAC conductance was specific for tubulin-dependent blockage of conductance, since erastin had no effect on conductance in the absence of tubulin. Normalized conductance *versus* voltage plots confirmed that erastin reverses and abrogates enhancement of VDAC voltage gating by tubulin (Fig. 6*B*).

DISCUSSION

Despite the aerobic glycolysis of Warburg metabolism in cancer cells, tumor mitochondria are functional and produce ATP by oxidative phosphorylation (7, 37). Except for a few membrane-permeant lipophilic compounds, such as molecular oxygen, virtually all metabolites that enter and leave mitochondria must cross the mitochondrial outer membrane through VDAC (32, 38, 39). Although generally considered to be constitutively open during metabolism to allow free diffusion of metabolites across the outer membrane, recent data suggests that VDAC can close physiologically to inhibit exchange of metabolites between mitochondria and the cytosol (9, 11, 21, 24, 40). Here, our findings show that knockdown of VDAC decreases $\Delta\Psi$ and that the magnitude of decrease is different depending on the VDAC isoform(s) knocked down (Figs. 1, *C* and *D* and 3, *A*–*D*). These findings support the conclusion that VDAC is limiting for metabolite exchange and $\Delta\Psi$ formation in HepG2 human hepatoma cells.

In Hela cells and in PC-12 cells, VDAC1 and VDAC2 are the most abundant isoforms and VDAC3 is a minor isoform as assessed by qPCR (41, 42). Our results using a different cell line, HepG2, showed also that VDAC 1 and 2 are the major VDAC isoforms (40 and 49%, respectively) followed by VDAC3 (11%).

Unexpectedly, knockdown of the minor isoform, VDAC3, produced the greatest decrease of $\Delta\Psi$ compared with other isoform knockdowns. Knockdown of VDAC3 but not of VDAC1 and VDAC2 also significantly decreased ATP, ADP, total adenine nucleotides, energy charge, phosphorylation potential, and NAD(P)H/NAD(P)$^+$ ratio (Fig. 2, *A*–*F*). An implication of these findings is that VDAC1 and VDAC2 are mostly closed in HepG2 cells, whereas the less abundant VDAC3 remains open, which would account for the greater effects of VDAC3 knockdown on mitochondrial metabolism and $\Delta\Psi$ formation.

Previously, we showed that free tubulin dynamically modulates $\Delta\Psi$ in cancer cells and proposed that the inverse relationship between cytosolic free tubulin levels and mitochondrial $\Delta\Psi$ is due to inhibition of VDAC by free tubulin, a proposal based on earlier findings that free tubulin blocks VDAC reconstituted into planar lipid bilayers and suppresses respiration of isolated mitochondria and permeabilized cells (24, 25, 43).

Consistent with our findings, paclitaxel but not nocodazole causes increases in respiration and production of reactive oxygen species, leading to release of cytochrome *c*. Paclitaxel is also proposed to promote opening of the permeability transition pores without having a direct effect on the respiratory chain. Whether increased respiration after paclitaxel is due to an uncoupling effect is controversial (44–46). Our results suggest that paclitaxel is promoting respiration through VDAC opening.

In the present study to show that VDAC deficiency causes $\Delta\Psi$ to decrease, single and double knockdowns of VDAC1, VDAC2, and VDAC3 were performed in all possible combinations. Findings from these knockdown experiments indicated that the greatest decrease of $\Delta\Psi$, the highest response to nocodazole and the lowest response to paclitaxel occurred after VDAC3 knockdown alone and after double knockdowns of VDAC1/3 or VDAC2/3 (Fig. 3, *A*–*D*). These observations led to the hypothesis that endogenous tubulin inhibits VDAC1 and VDAC2 conductance more than VDAC3 conductance and that VDAC3 is constitutively in a more open state than VDAC1 and VDAC2. Accordingly by this hypothesis in intact HepG2 cells, increases of free tubulin by agents like nocodazole have a relatively larger effect on VDAC3 because VDAC1 and VDAC2 are already closed by tubulin under baseline conditions. By contrast, paclitaxel which decreases free tubulin has a small effect on VDAC3 because endogenous free tubulin in the intact cells is causing little inhibition of VDAC3.

Studies using mouse VDAC expressed in VDAC deficient yeast show that VDAC1 and VDAC2 can each insert into phospholipid membranes and form channels with single-channel conductance, voltage dependence and ion selectivity established previously as characteristic of VDAC (47, 48). By contrast, VDAC3 does not insert easily in planar phospholipid bilayers and does not show characteristic gating at high membrane potentials (48). Yeast lacking endogenous VDAC have dysfunctional mitochondrial metabolism and lose the capacity to grow in non-fermentable medium. Expression of human and mouse VDAC1 or VDAC2 restores growth in non-fermentable medium and mitochondrial function, whereas VDAC3 reversed the VDAC-deficient phenotype much less efficiently (41, 47). VDAC1 knock-out mice are viable with only slightly affected mitochondrial function, whereas VDAC2 gene deletion is embryologically lethal (49, 50). Mice lacking VDAC3 have male infertility but are otherwise healthy (51). Such observations have called into question whether VDAC3 forms functional channels in the mitochondrial outer membrane. Here, we show that VDAC3 appears to be open in intact cells and that VDAC forms functional channels in planar lipid bilayers with characteristic voltage gating. Poor channel function of VDAC3 in previous studies expressing VDAC3 in yeast or overexpressing VDAC3 in mammalian cells (41) may indicate that post-translational modifications are required for proper VDAC3 functioning which may be missing in these models.

To better characterize the properties of the individual human VDAC isoforms, VDAC was isolated from HepG2 cells and inserted into planar lipid bilayers. For VDAC isolated from HepG2 cells not treated with siRNA, single-channel conductance, voltage-gating and blockage by dimeric tubulin were virtually identical to VDAC isolated from other sources, such as liver and heart mitochondria (supplemental Fig. S3). VDAC was also isolated from double knockdown HepG2 cells and inserted in lipid bilayers. Of the three isoforms, VDAC1 was the most sensitive to tubulin inhibition with VDAC2 almost equally sensitive. By contrast, tubulin even at 5-fold higher concentration had little effect on VDAC3 (Fig. 4*C*). Overall, these results are consistent with the conclusion that VDAC3 does indeed function as a channel in the outer membrane and is

constitutively open in proliferating HepG2 cells, whereas VDAC1 and VDAC2 are mostly blocked by tubulin, as we had inferred from measurement of various mitochondrial parameters in intact HepG2 cells made deficient of the VDAC isoforms in various combinations. To assess further tubulin-dependent control of VDAC conductance and mitochondrial $\Delta\Psi$ formation, we evaluated erastin, a VDAC-targeting small molecule lethal in some cancer cell lines. Erastin increased $\Delta\Psi$ in HepG2 cells and both blocked and reversed depolarization induced by colchicine and nocodazole (Fig. 5). These findings implied that erastin antagonizes the effects of free tubulin on VDAC conductance. To test this hypothesis directly, erastin was evaluated in VDAC reconstituted into planar lipid bilayers. In this experimental setting also, erastin both blocked and reversed the inhibition of VDAC conductance by dimeric free tubulin (Fig. 6). Future experiments will be needed to determine whether cell death induction by erastin is related to opening of VDAC channels.

In conclusion, our findings indicate that VDAC is an adjustable limiter (governator) of mitochondrial metabolism in HepG2 cells whose partial closure acts as a brake restricting mitochondrial $\Delta\Psi$ generation, oxidative metabolism and NAD(P)H generation. VDAC blockage, which is most marked for VDAC1 and VDAC2 isoforms, is caused by high free tubulin levels in proliferating cancer cells compared with non-transformed cells (*e.g.* hepatoma *versus* hepatocytes, see (9). Using VDAC3 from VDAC1/2 double knockdown HepG2 cells reconstituted into planar phospholipid bilayers, our findings also indicate that VDAC3 indeed does form functional channels that share the electrophysiological and functional characteristics of VDAC1 and VDAC2 with the exception of much smaller sensitivity to tubulin inhibition. The small anti-cancer molecule, erastin, antagonized inhibition of VDAC by tubulin. Thus, interference of interactions of tubulin with VDAC represents a new target for drug discovery, since drugs antagonizing this interaction, such as erastin, might lead to reversion of Warburg metabolism to the metabolism of non-cancerous cells with consequent anti-proliferative effect.

REFERENCES

1. Warburg, O., Wind, F., and Negelein, E. (1927) The Metabolism of Tumors in the Body. *J. Gen. Physiol* **8,** 519–530
2. Warburg, O. (1956) On the origin of cancer cells. *Science* **123,** 309–314
3. Gambhir, S. S. (2002) Molecular imaging of cancer with positron emission tomography. *Nat. Rev. Cancer* **2,** 683–693
4. Vander Heiden, M. G., Cantley, L. C., and Thompson, C. B. (2009) Understanding the Warburg effect: the metabolic requirements of cell proliferation. *Science* **324,** 1029–1033
5. Bonnet, S., Archer, S. L., Allalunis-Turner, J., Haromy, A., Beaulieu, C., Thompson, R., Lee, C. T., Lopaschuk, G. D., Puttagunta, L., Bonnet, S., Harry, G., Hashimoto, K., Porter, C. J., Andrade, M. A., Thebaud, B., and Michelakis, E. D. (2007) A mitochondria-K+ channel axis is suppressed in cancer and its normalization promotes apoptosis and inhibits cancer growth. *Cancer Cell* **11,** 37–51
6. Mathupala, S. P., Ko, Y. H., and Pedersen, P. L. (2009) Hexokinase-2 bound to mitochondria: cancer's stygian link to the "Warburg Effect" and a pivotal target for effective therapy. *Semin. Cancer Biol.* **19,** 17–24
7. Pedersen, P. L. (2007) Warburg, me and Hexokinase 2: Multiple discoveries of key molecular events underlying one of cancers' most common phenotypes, the "Warburg Effect", i.e., elevated glycolysis in the presence of oxygen. *J. Bioenerg. Biomembr.* **39,** 211–222
8. Nakashima, R. A., Paggi, M. G., and Pedersen, P. L. (1984) Contributions of glycolysis and oxidative phosphorylation to adenosine 5′-triphosphate production in AS-30D hepatoma cells. *Cancer Res.* **44,** 5702–5706
9. Maldonado, E. N., Patnaik, J., Mullins, M. R., and Lemasters, J. J. (2010) Free tubulin modulates mitochondrial membrane potential in cancer cells. *Cancer Res.* **70,** 10192–10201
10. Gellerich, F. N., Wagner, M., Kapischke, M., Wicker, U., and Brdiczka, D. (1993) Effect of macromolecules on the regulation of the mitochondrial outer membrane pore and the activity of adenylate kinase in the intermembrane space. *Biochim. Biophys. Acta* **1142,** 217–227
11. Hodge, T., and Colombini, M. (1997) Regulation of metabolite flux through voltage-gating of VDAC channels. *J. Membr. Biol.* **157,** 271–279
12. Lee, A. C., Zizi, M., and Colombini, M. (1994) Beta-NADH decreases the permeability of the mitochondrial outer membrane to ADP by a factor of 6. *J. Biol. Chem.* **269,** 30974–30980
13. Rostovtseva, T., and Colombini, M. (1997) VDAC channels mediate and gate the flow of ATP: implications for the regulation of mitochondrial function. *Biophys. J.* **72,** 1954–1962
14. Bayrhuber, M., Meins, T., Habeck, M., Becker, S., Giller, K., Villinger, S., Vonrhein, C., Griesinger, C., Zweckstetter, M., and Zeth, K. (2008) Structure of the human voltage-dependent anion channel. *Proc. Natl. Acad. Sci. U.S.A.* **105,** 15370–15375
15. Hiller, S., Garces, R. G., Malia, T. J., Orekhov, V. Y., Colombini, M., and Wagner, G. (2008) Solution structure of the integral human membrane protein VDAC-1 in detergent micelles. *Science* **321,** 1206–1210
16. Ujwal, R., Cascio, D., Colletier, J. P., Faham, S., Zhang, J., Toro, L., Ping, P., and Abramson, J. (2008) The crystal structure of mouse VDAC1 at 2.3 A resolution reveals mechanistic insights into metabolite gating. *Proc. Natl. Acad. Sci. U.S.A.* **105,** 17742–17747
17. Colombini, M. (1980) Structure and mode of action of a voltage dependent anion-selective channel (VDAC) located in the outer mitochondrial membrane. *Ann. N.Y. Acad. Sci.* **341,** 552–563
18. Colombini, M., Yeung, C. L., Tung, J., and König, T. (1987) The mitochondrial outer membrane channel, VDAC, is regulated by a synthetic polyanion. *Biochim. Biophys. Acta* **905,** 279–286
19. Mannella, C. A., Forte, M., and Colombini, M. (1992) Toward the molecular structure of the mitochondrial channel, VDAC. *J. Bioenerg. Biomembr.* **24,** 7–19
20. Song, J., and Colombini, M. (1996) Indications of a common folding pattern for VDAC channels from all sources. *J. Bioenerg. Biomembr.* **28,** 153–161
21. Lemasters, J. J., and Holmuhamedov, E. (2006) Voltage-dependent anion channel (VDAC) as mitochondrial governator–thinking outside the box. *Biochim. Biophys. Acta* **1762,** 181–190
22. Maldonado, E. N., and Lemasters, J. J. (2012) Warburg revisited: regulation of mitochondrial metabolism by voltage-dependent anion channels in cancer cells. *J. Pharmacol. Exp. Ther.* **342,** 637–641
23. Gurnev, P. A., Rostovtseva, T. K., and Bezrukov, S. M. (2011) Tubulin-blocked state of VDAC studied by polymer and ATP partitioning. *FEBS Lett.* **585,** 2363–2366
24. Rostovtseva, T. K., Sheldon, K. L., Hassanzadeh, E., Monge, C., Saks, V., Bezrukov, S. M., and Sackett, D. L. (2008) Tubulin binding blocks mitochondrial voltage-dependent anion channel and regulates respiration. *Proc. Natl. Acad. Sci. U.S.A.* **105,** 18746–18751
25. Timohhina, N., Guzun, R., Tepp, K., Monge, C., Varikmaa, M., Vija, H., Sikk, P., Kaambre, T., Sackett, D., and Saks, V. (2009) Direct measurement of energy fluxes from mitochondria into cytoplasm in permeabilized cardiac cells in situ: some evidence for Mitochondrial Interactosome. *J. Bioenerg. Biomembr.* **41,** 259–275
26. Lemasters, J. J., Holmuhamedov, E. L., Czerny, C., Zhong, Z., and Maldonado, E. N. (2012) Regulation of mitochondrial function by voltage dependent anion channels in ethanol metabolism and the Warburg effect. *Biochim. Biophys. Acta* **1818,** 1536–1544
27. Yagoda, N., von, Rechenberg, M., Zaganjor, E., Bauer, A. J., Yang, W. S., Fridman, D. J., Wolpaw, A. J., Smukste, I., Peltier, J. M., Boniface, J. J., Smith, R., Lessnick, S. L., Sahasrabudhe, S., and Stockwell, B. R. (2007) RAS-RAF-MEK-dependent oxidative cell death involving voltage-dependent anion channels. *Nature* **447,** 864–868

28. Bauer, A. J., Gieschler, S., Lemberg, K. M., McDermott, A. E., and Stockwell, B. R. (2011) Functional model of metabolite gating by human voltage-dependent anion channel 2. *Biochemistry* **50,** 3408–3410
29. Lemasters, J. J., and Ramshesh, V. K. (2007) Imaging of mitochondrial polarization and depolarization with cationic fluorophores. *Methods Cell Biol.* **80,** 283–295
30. Patterson, G. H., Knobel, S. M., Arkhammar, P., Thastrup, O., and Piston, D. W. (2000) Separation of the glucose-stimulated cytoplasmic and mitochondrial NAD(P)H responses in pancreatic islet beta cells. *Proc. Natl. Acad. Sci. U.S.A.* **97,** 5203–5207
31. Moran, U., Phillips, R., and Milo, R. (2010) SnapShot: key numbers in biology. *Cell* **141,** 1262
32. Rostovtseva, T. K., Kazemi, N., Weinrich, M., and Bezrukov, S. M. (2006) Voltage gating of VDAC is regulated by nonlamellar lipids of mitochondrial membranes. *J. Biol. Chem.* **281,** 37496–37506
33. Colombini, M. (1989) Voltage gating in the mitochondrial channel, VDAC. *J. Membr. Biol.* **111,** 103–111
34. Zizi, M., Byrd, C., Boxus, R., and Colombini, M. (1998) The voltage-gating process of the voltage-dependent anion channel is sensitive to ion flow. *Biophys. J.* **75,** 704–713
35. Nieminen, A. L., Byrne, A. M., Herman, B., and Lemasters, J. J. (1997) Mitochondrial permeability transition in hepatocytes induced by t-BuOOH: NAD(P)H and reactive oxygen species. *Am. J. Physiol.* **272,** C1286–C1294
36. Sies, H., and Gerstenecker, C. (1972) Oxidation in the NADP system and release of GSSG from hemoglobin-free perfused rat liver during peroxidatic oxidation of glutathione by hydroperoxides. *FEBS Lett.* **27,** 171–175
37. Weinberg, F., and Chandel, N. S. (2009) Mitochondrial metabolism and cancer. *Ann. N.Y. Acad. Sci.* **1177,** 66–73
38. Colombini, M. (2004) VDAC: the channel at the interface between mitochondria and the cytosol. *Mol. Cell Biochem.* **256–257,** 107–115
39. Rostovtseva, T. K., and Bezrukov, S. M. (2008) VDAC regulation: role of cytosolic proteins and mitochondrial lipids. *J. Bioenerg. Biomembr.* **40,** 163–170
40. Shoshan-Barmatz, V., De Pinto, V, Zweckstetter, M., Raviv, Z., Keinan, N., and Arbel, N. (2010) VDAC, a multi-functional mitochondrial protein regulating cell life and death. *Mol. Aspects Med.* **31,** 227–285
41. De Pinto, V., Guarino, F., Guarnera, A., Messina, A., Reina, S., Tomasello, F. M., Palermo, V., and Mazzoni, C. (2010) Characterization of human VDAC isoforms: a peculiar function for VDAC3? *Biochim. Biophys. Acta* **1797,** 1268–1275
42. Prins, J. M., Park, S., and Lurie, D. I. (2010) Decreased expression of the voltage-dependent anion channel in differentiated PC-12 and SH-SY5Y cells following low-level Pb exposure. *Toxicol. Sci.* **113,** 169–176
43. Monge, C., Beraud, N., Kuznetsov, A. V., Rostovtseva, T., Sackett, D., Schlattner, U., Vendelin, M., and Saks, V. A. (2008) Regulation of respiration in brain mitochondria and synaptosomes: restrictions of ADP diffusion in situ, roles of tubulin, and mitochondrial creatine kinase. *Mol. Cell Biochem.* **318,** 147–165
44. André, N., Braguer, D., Brasseur, G., Gonçalves, A., Lemesle-Meunier, D., Guise, S., Jordan, M. A., and Briand, C. (2000) Paclitaxel induces release of cytochrome c from mitochondria isolated from human neuroblastoma cells. *Cancer Res.* **60,** 5349–5353
45. André, N., Carré, M., Brasseur, G., Pourroy, B., Kovacic, H., Briand, C., and Braguer, D. (2002) Paclitaxel targets mitochondria upstream of caspase activation in intact human neuroblastoma cells. *FEBS Lett.* **532,** 256–260
46. Hu, Y., Moraes, C. T., Savaraj, N., Priebe, W., and Lampidis, T. J. (2000) Rho(0) tumor cells: a model for studying whether mitochondria are targets for rhodamine 123, doxorubicin, and other drugs. *Biochem. Pharmacol.* **60,** 1897–1905
47. Craigen, W. J., and Graham, B. H. (2008) Genetic strategies for dissecting mammalian and Drosophila voltage-dependent anion channel functions. *J. Bioenerg. Biomembr.* **40,** 207–212
48. Xu, X., Decker, W., Sampson, M. J., Craigen, W. J., and Colombini, M. (1999) Mouse VDAC isoforms expressed in yeast: channel properties and their roles in mitochondrial outer membrane permeability. *J. Membr. Biol.* **170,** 89–102
49. Anflous, K., Armstrong, D. D., and Craigen, W. J. (2001) Altered mitochondrial sensitivity for ADP and maintenance of creatine-stimulated respiration in oxidative striated muscles from VDAC1-deficient mice. *J. Biol. Chem.* **276,** 1954–1960
50. Cheng, E. H., Sheiko, T. V., Fisher, J. K., Craigen, W. J., and Korsmeyer, S. J. (2003) VDAC2 inhibits BAK activation and mitochondrial apoptosis. *Science* **301,** 513–517
51. Sampson, M. J., Decker, W. K., Beaudet, A. L., Ruitenbeek, W., Armstrong, D., Hicks, M. J., and Craigen, W. J. (2001) Immotile sperm and infertility in mice lacking mitochondrial voltage-dependent anion channel type 3. *J. Biol. Chem.* **276,** 39206–39212